Journal of Sound and Vibration (2001) **246**(2), 225–244
doi:10.1006/jsvi.2001.3634, available online at http://www.idealibrary.com on IDEAL®

HIERARCHICAL FINITE ELEMENT ANALYSES OF GEOMETRICALLY NON-LINEAR VIBRATION OF BEAMS AND PLANE FRAMES

P. RIBEIRO

DEMEGI, Faculdade de Engenharia, Universidade do Porto, Rua Dr. Roberto Frias, 4200-465 *Porto, Portugal. E-mail: pmleal@fe.up.pt*

(*Received* 9 *March* 2000, *and in final form* 18 *December* 2000)

Geometrically non-linear vibrations of beams and plane frameworks are analyzed by the hierarchical finite element method (HFEM). Two main points are of interest. The first is to compare polynomials, trigonometric functions and beam eigenfunctions as displacement shape functions for beam hierarchical finite elements. The second is to examine the suitability of the HFEM for time domain non-linear analyses.

1. INTRODUCTION

A structure subjected to large loads, or to loads with a frequency component close to a natural frequency, may undergo oscillations with large amplitudes, and thus with geometrical non-linearity. The beam is a widely used structural element, common in aerospace, civil and mechanical engineering structures. It can be used on its own, assembled to other beams, or to reinforce other elements such as plates or shells.

The finite element method (FEM) is a powerful means of structural analysis. In large amplitude vibrations, the FEM non-linear stiffness matrices are functions of the unknown generalized displacements. Therefore, in dynamic analysis in the time domain, iterations must be carried out in each time step, and in the frequency domain, for each frequency. Hence, substantial computational effort is required to complete a non-linear dynamic analysis using a model with a large number of degrees of freedom (d.o.f.).

In the *p*-version of the FEM, the accuracy of the approximation is improved by increasing the number of shape functions over the elements, without altering the mesh. Often, the set of functions of an approximation of lower order *p*, constitutes a subset of the set of functions of the approximation of order $p + 1$, and the *p*-version of the FEM is called "hierarchical finite element method" (HFEM).

Polynomial functions are more common in finite element analyses. Regarding the HFEM, Legendre polynomials in the Rodrigues form are quite popular. They have, for example, been applied to linear analyses of plates in references [1–3] and to non-linear dynamic analyses of beams and plates in the frequency domain in reference [4–8]. In these references, it was shown that convergence is achieved with far fewer degrees of freedom in the HFEM than in the *h*-version of the FEM.

Since high order polynomials are ill conditioned [9], some researchers advised the use of trigonometric displacement shape functions [10–13]. Houmat [10] investigated linear plate

0022-460X/01/370225 + 20 $35.00/0

vibration by the HFEM and compared trigonometric shape functions with Legendre polynomials. The trigonometric HFEM was found to yield better accuracy with less d.o.f. for *s-s-s-s* and *s-f-s-f* plates (*s*, *f* and *c* stand for simply supported, free and clamped boundary conditions respectively). For fully clamped and for free plates both sets of shape functions yield the same accuracy with the same number of d.o.f. Leung and Chan [11] used polynomials and trigonometric functions to analyze linear vibrations of beams and plates and found that accuracy is achieved with a reduced number of shape functions. Beslin and Nicolas [12] proposed a set of hierarchical trigonometric functions to predict flexural motion of plate-like structures in the medium frequency range. Bardell *et al*. applied these functions to study linear vibrations of shells [13].

Beam eigenfunctions, exact solutions of the linear problem, are trigonometric and hyperbolic or only trigonometric, depending on the boundary conditions. Since the non-linear mode shape is either similar (though generally different) to a linear mode, or to a combination of linear modes [8], a beam element built with those eigenfunctions should require a reduced number of degrees of freedom for accuracy in dynamic analyses. Another advantage of these functions is that the linear stiffness matrices and the mass matrices are diagonal, therefore well conditioned and with several computational benefits.

The studies [9–13] where trigonometric shape functions were used, are all concerned with linear analyses. In this paper, the advantages of different shape functions in the analysis of geometrically non-linear vibrations of plane beams and frames are investigated. Beam eigenfunctions, trigonometric functions and polynomials are tested. The manipulation of these functions can be quite cumbersome and will be carried out using symbolic computation.

The number of d.o.f. necessary for accuracy is one of the main points of interest since it determines the time necessary to solve the non-linear equations of motion. Nevertheless, another important characteristic to compare is the time required to compute the element matrices when using the different sets of shape functions. This may be a determinant factor, particularly because the calculation of the non-linear matrices requires much more time then the calculation of the linear ones.

Time domain numerical integration schemes are very versatile and allow one to analyze the response of structures to periodic and non-periodic loads. However, a dynamic analysis applying time domain methods and a FEM model with a large number of degrees of freedom may take quite a long time. Consequently, applications of these techniques to analyze non-linear vibration are often restricted to a small time span and to particular external loads. Due to its relatively small number of degrees of freedom, HFEM models should be ideally suited to time domain simulations. This will also be ascertained in this paper.

The governing differential equations in the time domain are derived by applying the principle of virtual work, and solved by Newmark's method. The equations of motion in the frequency domain are obtained by applying the harmonic balance method and solved by a continuation method. The results of different HFEM models and of *h*-version of the FEM models are compared. Free vibrations and the response to different loads are investigated using time plots, phase planes and Poincaré sections.

2. EQUATIONS OF MOTION

Torsion free, plane bending vibrations of elastic and isotropic frames constituted by beams with small uniform thickness *h*, are of interest. The derivation of the beam element matrices essentially follows the procedure presented by Ribeiro and Petyt [8].

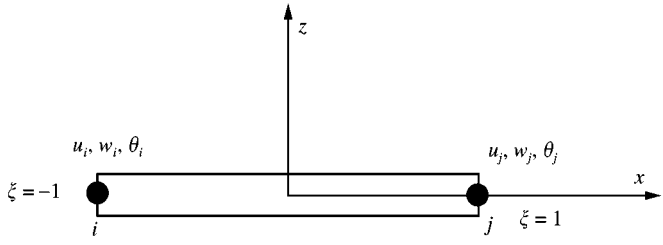

Figure 1. Beam element in local co-ordinate system.

The effects of transverse shear deformations and rotatory inertia are neglected, and the Bernoulli–Euler hypothesis is assumed. Therefore, the longitudinal displacement, u, and the transverse displacement, w, are given by

$$u(x, z, t) = u^0(x, t) - zw^0_{,x}, \qquad w(x, z, t) = w^0(x, t), \tag{1}$$

where u^0 and w^0 are the values of the longitudinal and transverse, or lateral, displacement components u and w at the middle plane and ",x" denotes the derivative with respect to x. $w^0_{,x}$ is the rotation of the cross-section about the y-axis. Assuming that the transverse deflection, w, is large compared with the beam thickness, but small compared with the length, L, of the beam, the following strain–displacement relationship results:

$$\varepsilon_x = u^0_{,x} + \tfrac{1}{2}(w^0_{,x})^2 - zw^0_{,xx}, \tag{2}$$

where $u^0_{,x} + \frac{1}{2}(w^0_{,x})^2$ is the non-linear longitudinal strain at the middle plane of the beam, and $w^0_{,xx}$ is the curvature of the beam.

A beam element is shown in Figure 1. ξ is a non-dimensional element, or local co-ordinate related to x by $\xi = 2x/L$.

The vector $\{\mathbf{d}\}$, formed by the displacement components at a point within the element, u and w, is expressed as the combination of the hierarchical shape functions and generalized displacements $\{\mathbf{q}\}$:

$$\{\mathbf{d}\} = \begin{Bmatrix} u \\ w \end{Bmatrix} = [\mathbf{N}]\{\mathbf{q}\}, \quad [\mathbf{N}] = \begin{bmatrix} \lfloor\, \mathbf{N}^u \,\rfloor & 0 \\ 0 & \lfloor\, \mathbf{N}^w \,\rfloor \end{bmatrix}, \tag{3, 4}$$

$$\lfloor\, \mathbf{N}^w \,\rfloor = \lfloor\, f_1(x)\ f_2(x)\ \cdots f_{p_0}(x) \,\rfloor, \tag{5}$$

$$\lfloor\, \mathbf{N}^u \,\rfloor = \lfloor\, g_1(x)\ g_2(x)\ \cdots g_{p_i}(x) \,\rfloor, \tag{6}$$

$$\{\mathbf{q}\}^{\mathrm{T}} = \lfloor\, \{\mathbf{q}_u\}^{\mathrm{T}}\ \{\mathbf{q}_w\}^{\mathrm{T}} \,\rfloor = \lfloor\, q_u(1)\ q_u(2)\ \cdots q_u(p_i)\ q_w(1)\ q_w(2)\ \cdots q_w(p_0) \,\rfloor, \tag{7}$$

where $[\mathbf{N}]$ is the matrix of shape functions, and $\lfloor\, \mathbf{N}^u \,\rfloor$ and $\lfloor\, \mathbf{N}^w \,\rfloor$ are, respectively, the longitudinal and the transverse shape function vectors. The vectors $\{\mathbf{q}_u\}$ and $\{\mathbf{q}_w\}$ are, respectively, the generalized displacement vectors in the x and z directions, p_i is the number of longitudinal shape functions and p_0 is the number of transverse shape functions used in the element.

The number of shape functions can vary from element to element. The element has six nodal degrees of freedom: two longitudinal displacements, $u_i = \{q_u(1)\}$ and $u_j = \{q_u(p_i)\}$; two transverse displacement, $w_i = \{q_v(1)\}$ and $w_j = \{q_v(p_0 - 1)\}$; and two rotations:

$\theta_i = \{q_v(2)\}$ and $\theta_j = \{q_v(p_0)\}$. These nodal degrees of freedom are used to enforce boundary conditions and continuity of displacements and rotations between elements (C_1 continuity). The other element degrees of freedom are internal to the element. In the HFEM only the shape functions that satisfy the geometric boundary conditions are included in the model.

It is worth pointing out that with this formulation the axial force can vary within the element. Often, particularly in analyses of slender beams, this force is approximated by its mean value over the element [14].

The principle of virtual work states that

$$\delta W_{in} + \delta W_V + \delta W_{ex} = 0, \tag{8}$$

where δW_{in}, δW_V and δW_{ex} are, respectively, the work done by the inertia, internal and external forces due to a virtual displacement $\{\delta d\}$.

Using d'Alembert's principle to define the virtual work of the inertia forces, the following expression for the element mass matrix $[\mathbf{M}]_e$ is obtained:

$$[\mathbf{M}]_e = \begin{bmatrix} [\mathbf{M}_p]_e & 0 \\ 0 & [\mathbf{M}_b]_e \end{bmatrix}$$

$$= \begin{bmatrix} \rho hb \int_L \lfloor\, \mathbf{N}^u \,\rfloor^{\mathrm{T}} \lfloor\, \mathbf{N}^u \,\rfloor \mathrm{d}L & 0 \\ 0 & \rho hb \int_L \lfloor\, \mathbf{N}^w \,\rfloor^{\mathrm{T}} \lfloor\, \mathbf{N}^w \,\rfloor \mathrm{d}L \end{bmatrix}, \tag{9}$$

where ρ is the mass per unit volume of the material that constitutes the beam element, b is the width of the element, and $[\mathbf{M}_p]_e$ and $[\mathbf{M}_b]_e$, are the longitudinal and bending mass matrices.

The element stiffness matrices are obtained from the work of the internal forces. The linear stiffness matrix $[\mathbf{K}_1]_e$ and the non-linear stiffness matrices $[\mathbf{K}_2]_e$, and $[\mathbf{K}_4]_e$ are defined by

$$[\mathbf{K}_1]_e = \begin{bmatrix} [\mathbf{K}_{1p}]_e & 0 \\ 0 & [\mathbf{K}_{1b}]_e \end{bmatrix}$$

$$= \begin{bmatrix} bhE \int_L \lfloor\, \mathbf{N}^u_{,x} \,\rfloor^{\mathrm{T}} \lfloor\, \mathbf{N}^u_{,x} \,\rfloor \mathrm{d}L & 0 \\ 0 & EI \int_L \lfloor\, \mathbf{N}^w_{,xx} \,\rfloor^{\mathrm{T}} \lfloor\, \mathbf{N}^w_{,xx} \,\rfloor \mathrm{d}L \end{bmatrix}, \tag{10}$$

$$[\mathbf{K}_2]_e = \left[\frac{1}{2} bhE \int_L (w_{,x}) \lfloor\, \mathbf{N}^u_{,x} \,\rfloor^{\mathrm{T}} \lfloor\, \mathbf{N}^w_{,x} \,\rfloor \mathrm{d}L \right], \tag{11}$$

$$[\mathbf{K}_4]_e = \left[\frac{1}{2} bEh \int_L \lfloor\, \mathbf{N}^w_{,x} \,\rfloor^{\mathrm{T}} \lfloor\, \mathbf{N}^w_{,x} \,\rfloor (w_{,x})^2 \mathrm{d}L \right]. \tag{12}$$

Matrices $[\mathbf{K}_{1p}]_e$ and $[\mathbf{K}_{1b}]_e$ are the longitudinal and bending linear stiffness matrices. Matrices $[\mathbf{K}_3]_e$ and $[\mathbf{K}_2]_e$ are related by $[\mathbf{K}_3]_e = 2[\mathbf{K}_2]_e^{\mathrm{T}}$. E is the Young modulus and I is the second moment of area of the cross-section of the beam element.

If $P_{0j}(t)$ represents a concentrated transverse force acting at the point $x = x_j$, $P_{0d}(x, t)$ a transverse distributed force, $P_{\ell j}(t)$ a concentrated longitudinal force acting at the point $x = x_j$, and $P_{\ell d}(x, t)$ a longitudinal distributed force, the virtual work of the external forces is

given by

$$\delta W_{ex} = \int_L [P_{0j}(t)\,\delta(x - x_j) + P_{0d}(x, t)]\,\delta w(x, t)\,\mathrm{d}L$$

$$+ \int_L [P_{\ell j}(t)\,\delta(x - x_j) + P_{\ell d}(x, t)]\,\delta u(x, t)\,\mathrm{d}L = \{\delta \mathbf{q}_w\}^{\mathrm{T}}\{\mathbf{P}_w(t)\}_e + \{\delta \mathbf{q}_p\}^{\mathrm{T}}\{\mathbf{P}_p(t)\}_e, \quad (13)$$

where $\{\mathbf{P}_w(t)\}_e$ and $\{\mathbf{P}_p(t)\}_e$ are the element vectors of generalized external forces applied in, respectively, the transverse and longitudinal directions and $\delta(x - x_j)$ is a spatial Dirac delta function.

Beams are analyzed with one hierarchical finite element only. In order to analyze plane frames the following procedure is adopted:

(1) one element is assigned to each bar of the frame;
(2) the number of shape functions to use in each element is chosen;
(3) the element matrices are calculated;
(4) the nodal degrees of freedom are transformed from local to global axes and the element matrices in the global co-ordinate system are calculated;
(5) the element matrices are assembled into global matrices.

The procedures applied in steps (4) and (5) are similar to the one applied in the usual FEM [15]. For example, the mass matrix in global co-ordinates, $[\bar{\mathbf{M}}]_e$, is given by

$$[\bar{\mathbf{M}}]_e = [\mathbf{R}]_e^{\mathrm{T}}[\mathbf{M}]_e[\mathbf{R}]_e, \quad (14)$$

where $[\mathbf{R}]_e$ is the matrix of direction cosines. This matrix transforms the generalized co-ordinates from global to local axes:

$$\{\mathbf{q}\}_e = [\mathbf{R}]_e\{\bar{\mathbf{q}}\}_e. \quad (15)$$

The bar over the vectors and matrices indicates that these are related to global co-ordinates.

The co-ordinates linked with the hierarchical shape functions are internal to each element, and therefore the part of the element matrices strictly associated with them is not altered in steps (4) and (5).

Although it is quite common to use hysteretic damping in finite element analyses, it should not be used in time domain studies, because it does not respect the causality principle [16]. Thus, stiffness proportional viscous damping, with a damping parameter α, is added to the equations of motion, and the following two coupled systems of equations of motion are obtained:

$$[\bar{\mathbf{M}}_p]\{\ddot{\bar{\mathbf{q}}}_p\} + \alpha[\bar{\mathbf{K}}_{1p}]\{\dot{\bar{\mathbf{q}}}_p\} + [\bar{\mathbf{K}}_{1p}]\{\bar{\mathbf{q}}_p\} + [\bar{\mathbf{K}}_2]\{\bar{\mathbf{q}}_w\} = \{\bar{\mathbf{P}}_p\}, \quad (16)$$

$$[\bar{\mathbf{M}}_b]\{\ddot{\bar{\mathbf{q}}}_w\} + \alpha[\bar{\mathbf{K}}_{1b}]\{\dot{\bar{\mathbf{q}}}_w\} + ([\bar{\mathbf{K}}_{1b}] + [\bar{\mathbf{K}}_4])\{\bar{\mathbf{q}}_w\} + [\bar{\mathbf{K}}_3]\{\bar{\mathbf{q}}_p\} = \{\bar{\mathbf{P}}_w\}. \quad (17)$$

The meaning of the matrices and vectors in the two former equations in similar to those of the element ones, but now they are expressed in global axes and correspond to the assembled model.

Since the longitudinal inertia was not neglected, the equations of motion have quadratic — $[\bar{\mathbf{K}}_2]\{\bar{\mathbf{q}}_w\}$ and $[\bar{\mathbf{K}}_3]\{\bar{\mathbf{q}}_p\}$ — and cubic — $[\bar{\mathbf{K}}_4]\{\bar{\mathbf{q}}_w\}$ — non-linearities and, therefore, they

are not equations of the Duffing type. The non-linear stiffness matrix

$$[\overline{\mathbf{KNL}}] = \begin{bmatrix} 0 & [\bar{\mathbf{K}}_2] \\ [\bar{\mathbf{K}}_3] & [\bar{\mathbf{K}}_4] \end{bmatrix} \tag{18}$$

is not symmetric.

Often, for slender beams, the longitudinal inertia and the damping contribution due to the longitudinal stress are negligible [17, 18]. In this case, $\{\bar{\mathbf{q}}_p\}$ can be eliminated from equations (16) and (17) and the equations of motion are simplified to equations of the Duffing type:

$$[\bar{\mathbf{M}}_b]\{\ddot{\bar{\mathbf{q}}}_w\} + \alpha[\bar{\mathbf{K}}_{1b}]\{\dot{\bar{\mathbf{q}}}_w\} + [\bar{\mathbf{K}}_{1b}]\{\bar{\mathbf{q}}_w\} + [\overline{\mathbf{K}nl}]\{\bar{\mathbf{q}}_w\} = -[\bar{\mathbf{K}}_3][\bar{\mathbf{K}}_{1p}]^{-1}\{\bar{\mathbf{P}}_p\} + \{\bar{\mathbf{P}}_w\}, \tag{19}$$

$$[\overline{\mathbf{K}nl}] = [\bar{\mathbf{K}}_4] - 2[\bar{\mathbf{K}}_2]^{\mathrm{T}}[\bar{\mathbf{K}}_{1p}]^{-1}[\bar{\mathbf{K}}_2], \tag{20}$$

Nevertheless, even small longitudinal forces can cause the longitudinal inertia to have some importance [19], and, in the presence of longitudinal forces, the longitudinal inertia will not be neglected. Therefore, it will always be taken into account in the analysis of frames.

The HBM relies upon assuming a time solution in the form of a Fourier series, and comparing the coefficients of the same harmonic components. In this way, non-linear differential equations in the space variables and frequency are obtained. In this paper, they are solved by a continuation method [8, 20]. The HBM will only be applied to compare results with published ones in harmonic vibration. Therefore, multi-modal vibrations will not be studied in the frequency domain (they will, though, be studied in the time domain). A frequency domain study of beam multi-modal vibration was carried out in reference [8].

The time domain equations of motion are solved by Newmark's direct integration method [15, 21], with Newmark parameters: $\gamma = \frac{1}{2}$ and $\beta = \frac{1}{4}$. With these parameters the method is also known as "average acceleration method". This is an implicit method, unconditionally stable for linear systems, but numerical instabilities can arise for non-linear systems and the energy of the system may be changed [21]. In order to minimize these effects, particular care was given to the choice of the time step in the examples presented in this paper. This was lower than the value recommended for linear systems, $\Delta t = \pi/50\omega_n$ [15], where ω_n is the natural frequency of the highest mode which contributes significantly to the response. Moreover, the validity of the results was verified by using different time steps.

3. DISPLACEMENT SHAPE FUNCTIONS

The performance of different sets of transverse shape functions will be investigated in this paper. One of these sets is constituted by the Rodrigues form of Legendre polynomials and by the cubic shape functions, known as Hermite cubics, usually applied in the *h*-version of the FEM [1–8, 10]. With this set, which is called the set of *f* shape functions, C^1 continuity exists between elements. Moreover, boundary conditions are easy to implement, since only one of the first four shape functions has either displacement or rotation different from zero at the end of each element. All higher order hierarchical functions have zero amplitudes and slopes at $\xi = -1$ and 1. A set of polynomials called the *g* set, which so far has only been

used as longitudinal shape functions, will also be applied in conjunction with Hermite cubics f_1 and f_3. With this set only C^0 continuity is guaranteed between elements. Both sets are given in Appendix A.

Beam eigenfunctions, i.e., the linear modes of bending vibration of a beam, will also be tried. These functions are trigonometric and hyperbolic or only trigonometric, depending on the boundary conditions, and can be found in some standard books on vibrations, as for example in reference [22]. It is worth pointing out here that the non-linear modes vary with the vibration amplitude and are not equal to the linear ones.

Trigonometric shape functions, which have been applied in references [12, 13] to study the linear vibrations of plates and of curved panels, and which have as an advantage over high order polynomials the fact that they are not ill conditioned, will be tested. They are also given in Appendix A. In order to satisfy boundary conditions, the functions f_1–f_4 are used in conjunction with the trigonometric functions.

Finally, a set of functions which is a variant of Houmat's functions [10] is also investigated. This set of functions is derived by assuming the following displacement field for the two-node beam element:

$$w = c_1 + c_2 + c_3 + c_4 + c_{r+4} \sin \frac{r\pi}{2}(\xi + 1), \quad r > 4. \tag{21}$$

Following the steps in reference [10], the ensuing set of hierarchical shape functions is derived:

$$H_{r+4} = \frac{r\pi}{8}[-(1-(-1)^r) + (1+(-1)^r)\xi + (1-(-1)^r)\xi^2 - (1-(-1)^r)\xi^3]$$

$$+ \sin \frac{r\pi}{2}(\xi + 1).$$

This set of functions leads to zero displacement and rotation at the element's nodes and is well conditioned. The first four shape functions are again the Hermite cubics.

Regarding longitudinal shape functions, the g polynomials and the bar eigenfunctions, exact solutions of linear longitudinal vibration of a beam (a problem usually called vibration of rods or bars), will be used. The latter are simply sine functions.

A symbolic computation package is employed to manipulate the shape functions and construct the element mass and stiffness matrices.

4. NUMERICAL RESULTS AND DISCUSSIONS

Simply supported and clamped–clamped beams, and two plane frames made of aluminium, with a Young modulus $E = 7 \times 10^{10}$ N/m^2 and mass density $\rho = 2778$ kg/m^3, are analyzed. The beams width, thickness and length are, respectively, $b = 0{\cdot}02$ m, $h = 0{\cdot}002$ m and $L = 0{\cdot}58$ m. The plane frames are constituted by three bars, as shown in Figure 2. The exterior boundary conditions are clamped, but in Frame 1, bar 2 is rigidly linked to bars 1 and 3, whilst in Frame 2 the bars are connected by articulated joints. The bars have equal square section, whose width is $b = 0{\cdot}02$ m, and equal length, $L = 0{\cdot}5$ m.

In the first subsection, the convergence with different sets of shape functions is analyzed in detail by studying harmonic free vibration in the frequency domain, and results are compared with published results. Then, in a second subsection, time domain analyses are carried out.

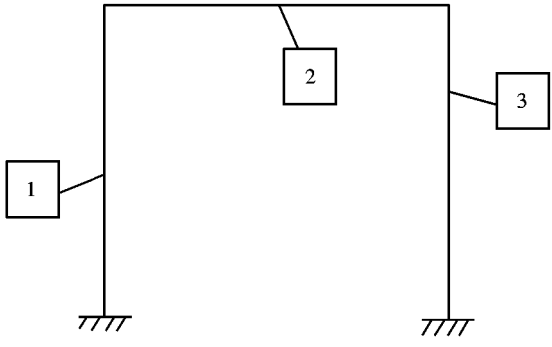

Figure 2. Portal plane frame.

The linear modes of a simply supported and a clamped–clamped beam are symmetric or antisymmetric. In the harmonic solution of beams, these symmetries are used to reduce the number of degrees of freedom of the model by an adequate choice of transverse and longitudinal shape functions. However, in non-harmonic vibration antisymmetric modes can be excited by symmetric ones and *vice versa* [8]. Therefore, in the time domain simulations, both symmetric and antisymmetric shape functions are used.

4.1. FREQUENCY DOMAIN ANALYSES—COMPARISON OF DIFFERENT SHAPE FUNCTIONS

This section begins with the analysis of simply supported beams. Table 1 compares the number of d.o.f. required to calculate the fundamental linear frequency in the *h*-versions of the FEM and the HFEM with different transverse shape functions. Obviously, with beam eigenfunctions, a number of linear modes equal to the number of shape functions used can be studied accurately. The polynomial g shape functions perform better than the f ones, since they respect the simply supported boundary conditions without the need to use the cubic polynomials f_2 and f_4. The *h*-versions of the FEM require more degrees of freedom than any HFEM one.

Regarding non-linear analyses, the convergence study shown in Table 2 demonstrates that a very small number of transverse and longitudinal beam eigenfunctions provides very accurate results (the relative error is always smaller than $2{\cdot}75 \times 10^{-4}$). w_m represents the maximum amplitude of vibration and r the radius of gyration.

In Table 3, the non-linear natural frequencies of vibration calculated using the beam eigenfunctions are compared with the ones calculated using polynomials, and with results from the literature. The HFEM with beam eigenfunctions requires a smaller number of degrees of freedom for accuracy: four f polynomials or three g polynomials are necessary to provide results that are slightly less accurate than with two beam eigenfunctions.

The number of degrees of freedom of the model has a great influence on the time necessary to calculate the solutions. However, the time necessary to compute the element matrices and obtain the model may also be an important factor in the choice of a set of shape functions. Table 4 compares the CPU time necessary to generate the hierarchical non-linear beam elements of Table 3 with different shape functions.[†] The time required when using beam eigenfunctions was taken as reference. The same two longitudinal shape

[†]It is important to point out that this analysis was carried out using symbolic computation and the same quite simple algorithm for all computations.

TABLE 1

Fundamental linear frequency parameter $\lambda = \omega_\ell^2 mL^4/EI$.*ss beam*

Exact [22]	FEM [23] (eight elements − 34 d.o.f.)	FEM [14] (six elements − 12 d.o.f.)	HFEM − f polynomials (1 el. − 4 d.o.f.)	HFEM − g polynomials (1 el. − 3 d.o.f.)	HFEM − beam eigenfunctions (1 el. − 1 d.o.f.)
97·409	97·409	97·419	97·409	97·409	97·409

m is the mass per unit length.

TABLE 2

Non-linear natural frequency $\omega/\omega_{\ell 1}$ *calculated with ss beam eigenfunctions*

$p_0 = 2$				$p_i = 4$			
w_m/r	$p_i = 1$	$p_i = 4$	$p_i = 8$	w_m/r	$p_0 = 1$	$p_0 = 2$	$p_0 = 4$
1·0	1·0897	1·0897	1·0897	1·0	1·0900	1·0897	1·0897
2·0	1·3229	1·3229	1·3229	2·0	1·3231	1·3229	1·3229
3·0	1·6394	1·6394	1·6394	3·0	1·6396	1·6394	1·6394

TABLE 3

Non-linear natural frequencies $\omega/\omega_{\ell 1}$ *of ss beam*

w_m/r	$\omega/\omega_{\ell 1}$ Elliptic integral [24]	$\omega/\omega_{\ell 1}$ HFEM f polynomials 4 d.o.f.	$\omega/\omega_{\ell 1}$ HFEM g polynomials 3 d.o.f.	$\omega/\omega_{\ell 1}$ HFEM eigenfunctions 2 d.o.f.	$\omega/\omega_{\ell 1}$ [14] six elements 12 d.o.f.
1·0	1·0892	1·0897	1·0897	1·0897	1·0865
2·0	1·3177	1·3229	1·3229	1·3299	1·3331
3·0	1·6256	1·6400	1·6398	1·6394	1·6422

TABLE 4

CPU time required to create different hierarchical elements for ss beam

	Transverse shape functions		
Longitudinal shape functions	f polynomials 4 d.o.f.	g polynomials 3 d.o.f.	Beam eigenfunctions 2 d.o.f.
Trigonometric	230%	85%	100%
polynomial	95%	68%	68%

functions were applied to calculate the result in each row. Since they require more shape functions for accuracy, f polynomials also require more computing time to construct the beam element. The set of g polynomials is the one that demands less time.

TABLE 5

Non-linear natural frequency, $\omega/\omega_{\ell 1}$ of cc beam. Beam eigenfunctions

	$p_0 = 2$			$p_i = 4$			$p_0 = 4$	
w_m/r	$p_i = 1$	$p_i = 2$	$p_i = 4$	$p_0 = 1$	$p_0 = 2$	$p_0 = 4$	$p_i = 5$	$p_i = 6$
1·0	1·0321	1·0225	1·0222	1·0223	1·0222	1·0222	1·0222	1·0222
2·0	1·1225	1·0873	1·0860	1·0863	1·0860	1·0860	1·0858	1·0858
3·0	1·2579	1·1875	1·1843	1·1853	1·1843	1·1839	1·1834	1·1833

TABLE 6

Linear natural frequencies of cc beam (rad/s)

	$\omega_{\ell 1}$	$\omega_{\ell 2}$	$\omega_{\ell 3}$	$\omega_{\ell 4}$
10 Legendre pol.	192·751	531·325	1041·61	1721·83
10 *H* functions	192·751	531·325	1041·61	1721·84
15 trigonometric functions	192·774	531·543	1042·30	1724·12

TABLE 7

Natural frequency, $\omega/\omega_{\ell 1}$, of cc beam

w_m/h	0·5	1	1·5	2
HFEM polynomials, 5 d.o.f. ($p_0 = 5$ and $p_i = 5$) [8]	1·0651	1·2377	1·4771	1·7530
HFEM eigenfunctions 4 d.o.f. ($p_0 = 4$ and $p_i = 5$)	1·0651	1·2379	1·4777	1·7550
HFEM eigenfunctions 5 d.o.f. ($p_0 = 5$ and $p_i = 6$)	1·0651	1·2377	1·4771	1·7534
w_m/r	1	2	3	—
FEM [25] – eight quadrilateral elements	1·0217	1·0831	1·1756	—
HFEM eigenfunctions 1 element 4 d.o.f. ($p_0 = 4$ and $p_i = 6$)	1·0222	1·0858	1·1833	—

Regarding clamped–clamped beams, Table 5 shows that a small number of transverse and longitudinal *cc* beam eigenfunctions provides an accurate calculation of the non-linear natural frequency. However, more shape functions are necessary than in the simply supported case.

The convergence of the linear natural frequencies is approximately as rapid with the *H* shape functions as with the Legendre polynomials (Table 6). The trigonometric shape functions did not behave very well at these lower frequencies: with 15 transverse shape functions, convergence had not yet been achieved.

In Table 7, the non-linear natural frequencies of vibration calculated by the HFEM with beam eigenfunctions are compared with the HFEM ones calculated in reference [8] using

TABLE 8

CPU time required to create hierarchical elements with 4 *d.o.f.* ($p_0 = 4$) *for cc beam*

	Polynomials	Eigenfunctions	Trigonometric functions	*H* functions
CPU time	0·33%	100%	40%	45%

polynomials and with the *h*-version of the FEM results given in reference [25]. The FEM requires more d.o.f. than any version of the HFEM. The table also shows that no visible gain results from using the beam shape functions instead of the Legendre polynomials, to study non-linear clamped–clamped beams.

Table 8 compares the CPU time necessary to generate hierarchical non-linear beam elements with different shape functions. Four transverse shape functions and two longitudinal shape functions were used in all cases. The longitudinal functions are polynomials in the first two columns and sine functions in the other two. The time required when using beam eigenfunctions was taken as reference.

The time necessary to construct the element matrices greatly increases with the number of *cc* beam eigenfunctions employed, because these are trigonometric and hyperbolic functions. If the same number of d.o.f. is used, the trigonometric shape functions suggested by Beslin and Nicolas [12] and the trigonometric *H* functions require less time than the *cc* beam eigenfunctions, but require much more time than Legendre polynomials. The same remains true if the *H* functions are used in conjunction with polynomial functions for the longitudinal displacements. As seen before, the Beslin and Nicolas functions require many more d.o.f. for an accurate investigation of low order modes than any of the other functions.

Modes of very high order were analyzed and no ill-conditioning problems were found with the high order Rodrigues' form of Legendre polynomials employed. Should these occur, then more elements can be added to the model and the order of the shape functions reduced. Otherwise, trigonometric functions may be used, and the set of *H* functions is recommended. Obviously, if modes of very high order are under study, then the Bernoulli–Euler theory is not valid and rotatory inertia and shear deformation should be taken into account.

Other polynomials did not behave as well as the Legendre ones. For example, a group of orthogonal polynomials presented by Bhat [26] were investigated by Ribeiro and Petyt in reference [27]. It was found that the Rodrigues form of Legendre polynomials permit a quicker derivation of the matrices involved in the HFEM. Moreover, it was numerically verified by analyzing isotropic beams that these polynomials produce diagonal linear longitudinal and bending stiffness matrices and a non-linear stiffness matrix with dominant diagonal terms. In the same case, Bhat's polynomials have the advantage of producing a diagonal mass matrix (with the other set of polynomials, the mass matrix is banded), which could allow a quicker resolution of eigenvalue problems and of the equations of motion. However, the non-linear stiffness matrix does not have a dominant diagonal and high order Bhat's polynomials are greatly affected by numerical errors, as shown in Figure 3.

In conclusion, for a general non-linear dynamic plane problem with beam elements, the best choice of shape functions seems to be the set of Legendre polynomials plus Hermite cubics for the transverse displacements and the *g* polynomials plus linear functions for the axial displacement. With these sets, different boundary conditions can be respected and C^1 continuity of transverse displacements is guaranteed between elements. Moreover, for non-linear vibration of clamped–clamped beams, Legendre polynomials display the same

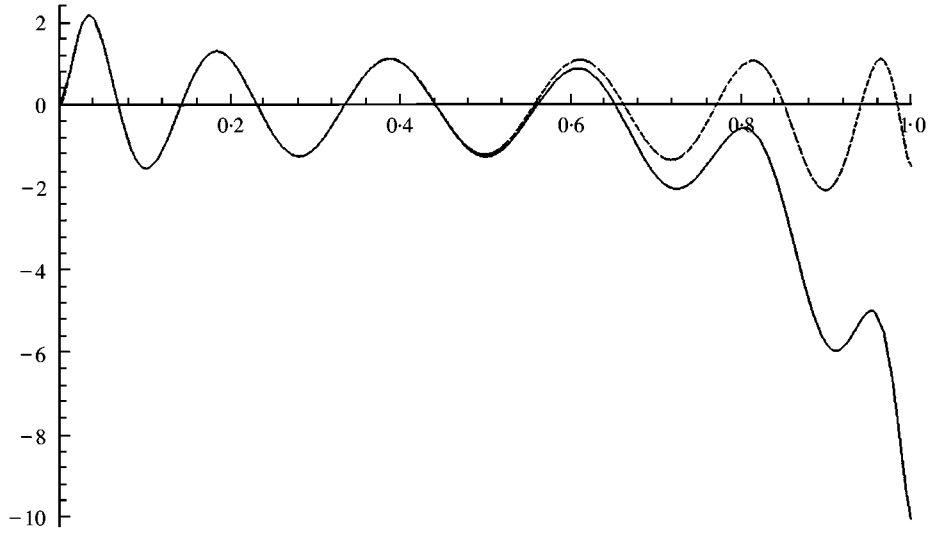

Figure 3. Bhat's polynomial of order 14: ——, plotted using nine digits; – – – –, plotted using 10 digits.

TABLE 9

First five linear natural frequencies of portal Frame 1 (*Hz*)

FEM			Polynomial HFEM		
177 d.o.f.	222 d.o.f.	357 d.o.f.	30 d.o.f.	34 d.o.f.	49 d.o.f.
58·955	58·955	58·955	59·103	59·103	59·103
231·56	231·56	231·56	232·69	232·69	232·69
377·23	377·23	377·23	380·47	380·47	380·47
405·84	405·83	405·83	410·39	410·38	410·38
811·96	811·93	811·90	823·74	823·66	823·66

or better degree of accuracy with similar number of degrees of freedom than the other sets of functions analyzed, and require far less time to compute the element matrices.

On the other hand, simply supported beam eigenfunctions, which are simply sine functions, allow the element matrices to be computed quickly, and require a reduced number of degrees of freedom. Nevertheless, with these latter functions continuity of rotation between elements cannot be guaranteed (only C^0 continuity is guaranteed). Therefore, sine functions are only recommended as transverse displacement shape functions if the problem has beam elements with simply supported boundary conditions. Another good option for this latter case is the set of g polynomials.

The frames were analyzed using three elements, one for each bar. Regarding Frame 1, the transverse shape functions used are the f polynomials. The longitudinal shape functions are the g polynomials.

In Table 9, the linear natural frequencies of Frame 1, calculated using the h-version of the finite element method, implemented in a commercial software package, and the HFEM are given. The results agree closely, although the HFEM converges to slightly larger values. With 34 d.o.f. the HFEM calculates the first five linear natural frequencies with five digit

TABLE 10

First five linear natural frequencies of portal Frame 2 (Hz)

FEM		Polyn./trigonometric HFEM		Polynomial HFEM	
224 d.o.f.	359 d.o.f.	24 d.o.f.	51 d.o.f.	37 d.o.f.	48 d.o.f.
37·170	37·170	37·201	37·201	37·201	37·201
181·12	181·12	181·62	181·62	181·62	181·62
282·34	282·34	284·19	284·19	284·19	284·19
309·62	309·62	311·77	311·77	311·77	311·77
712·60	712·58	720·18	720·18	720·18	720·18

accuracy, while the FEM with 222 d.o.f. (each bar is modelled by 25 elements) calculates the fifth natural frequency with only four digit accuracy.

In the *h*-version of the FEM model used, each element has 2 nodes and 3 degrees of freedom per node and several elements are necessary to model each bar. Therefore, continuity of the second derivative of the transverse displacement and first derivative of the axial displacement are not imposed between the elements. On the other hand, those continuities, and continuity of higher order derivatives, are always respected in each bar of the HFEM model, since a bar is represented by one element only with high order shape functions.

In Table 10, the linear natural frequencies of Frame 2, calculated using the *h*-version of the finite element method and the HFEM are given. Bars one and three were modelled using f polynomials. Bar three was modelled with g polynomials plus functions f_1 and f_3 (polynomial HFEM), or with sine functions plus functions f_1 and f_3 (polynomial/trigonometric HFEM). The results agree closely, but both HFEM models allow accurate results to be obtained with far fewer degrees of freedom then the *h*-version of the FEM. In this case, the HFEM with trigonometric shape functions is the one that requires less d.o.f.

4.2. TIME DOMAIN ANALYSES

A point harmonic excitation was applied transversely at the middle of the beam clamped at both ends. The frequency of the external force is 210 rad/s and its amplitude was varied from 1 to 10 N. The value of the damping parameter is 0·001, the longitudinal displacements were not neglected but the longitudinal inertia was.

In Figure 4, the phase plots and time histories of the response at the middle of the beam are represented for two amplitudes of excitation. The shapes assumed by the beam at four instants separated by a quarter of the period of excitation are also shown.

Since both phase plots are closed curves in the phase plane, the beam vibrates in a periodic manner. For larger amplitudes of the external force, the third mode of vibration is excited, harmonics other than the fundamental are present in the response and the phase plane loses symmetry with respect to the origin.

In order to assess the influence of the damping parameter a transverse force with 210 rad/s and 10 N was again applied to the *cc* beam, but now with α equal to 0·0001. In Figure 5, the phase plots, time histories and Poincaré maps of the response at the middle of the beam, and the shapes assumed by the beam at a particular instant are shown.

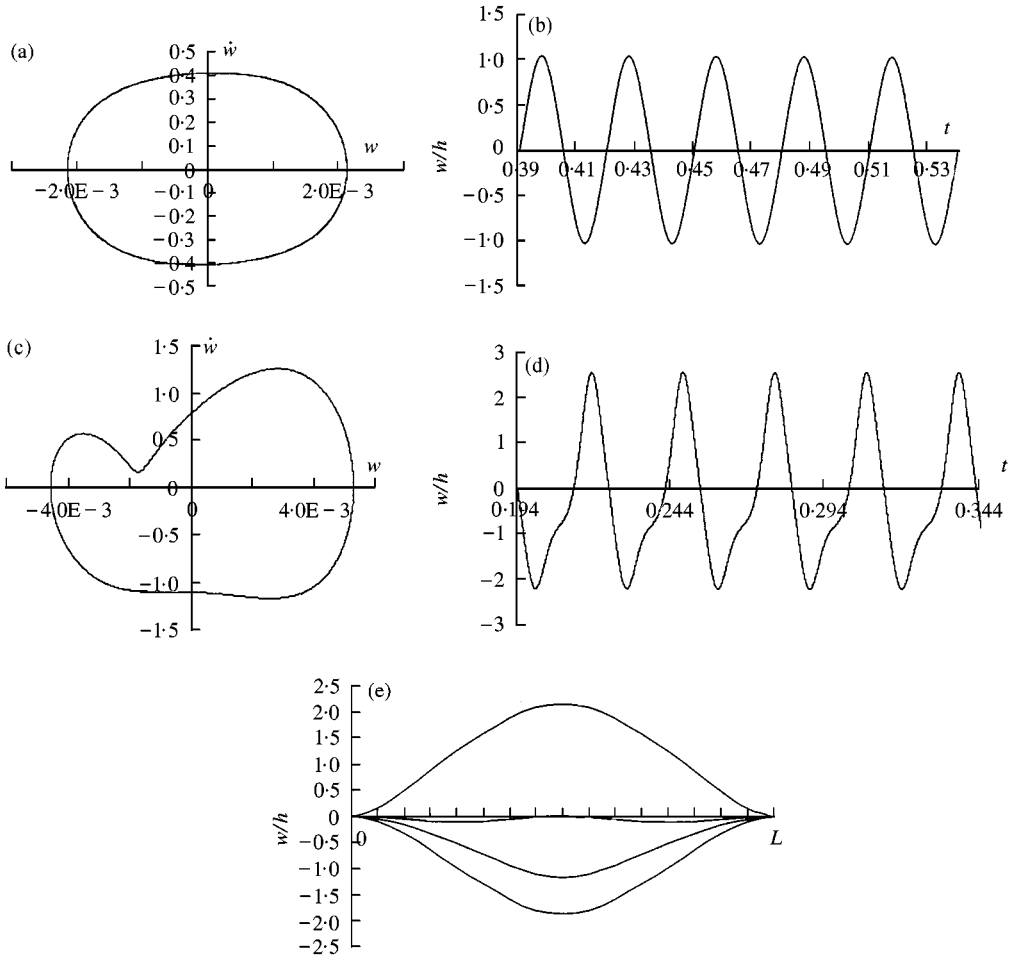

Figure 4. (a) Phase plot and (b) time history at the middle of the beam, when $F = 1$ N. (c) Phase plot and (d) time history at the middle of the beam, and (e) shapes assumed by the beam, when $F = 10$ N.

Plots (a), (c), (e) and (g) were obtained without longitudinal inertia and plots (b), (d), (f) and (h) with longitudinal inertia.

Although the frequency of excitation is close to the first linear natural frequency, the shape of the beam at the instant represented in Figure 5 is determined by the first and third modes. The Poincaré sections are defined by $w(\xi = 0) \cong -2{\cdot}55 \times 10^{-3}$. Since the orbit intersects the Poincaré sections twice, as shown in Figure 5(g) and 5(h), a period-doubling bifurcation occurred. The state-space portraits are closed lines and therefore the beam still vibrates in a periodic manner. Although the amplitude of vibration computed with and without considering the longitudinal inertia is the same, the plots show that this inertia has little influence on the response of the beam. The axial displacement and inertia will be taken into account in all of the following computations.

A transverse excitation of the form $F = 10\cos(210t) + 5\cos(225t)$ was applied at the middle of the beam clamped a both ends. In this and the following analyses the value of α is 0·0001. Figure 6 shows the phase plot, time history and Poincaré map of the response at the middle of the beam.

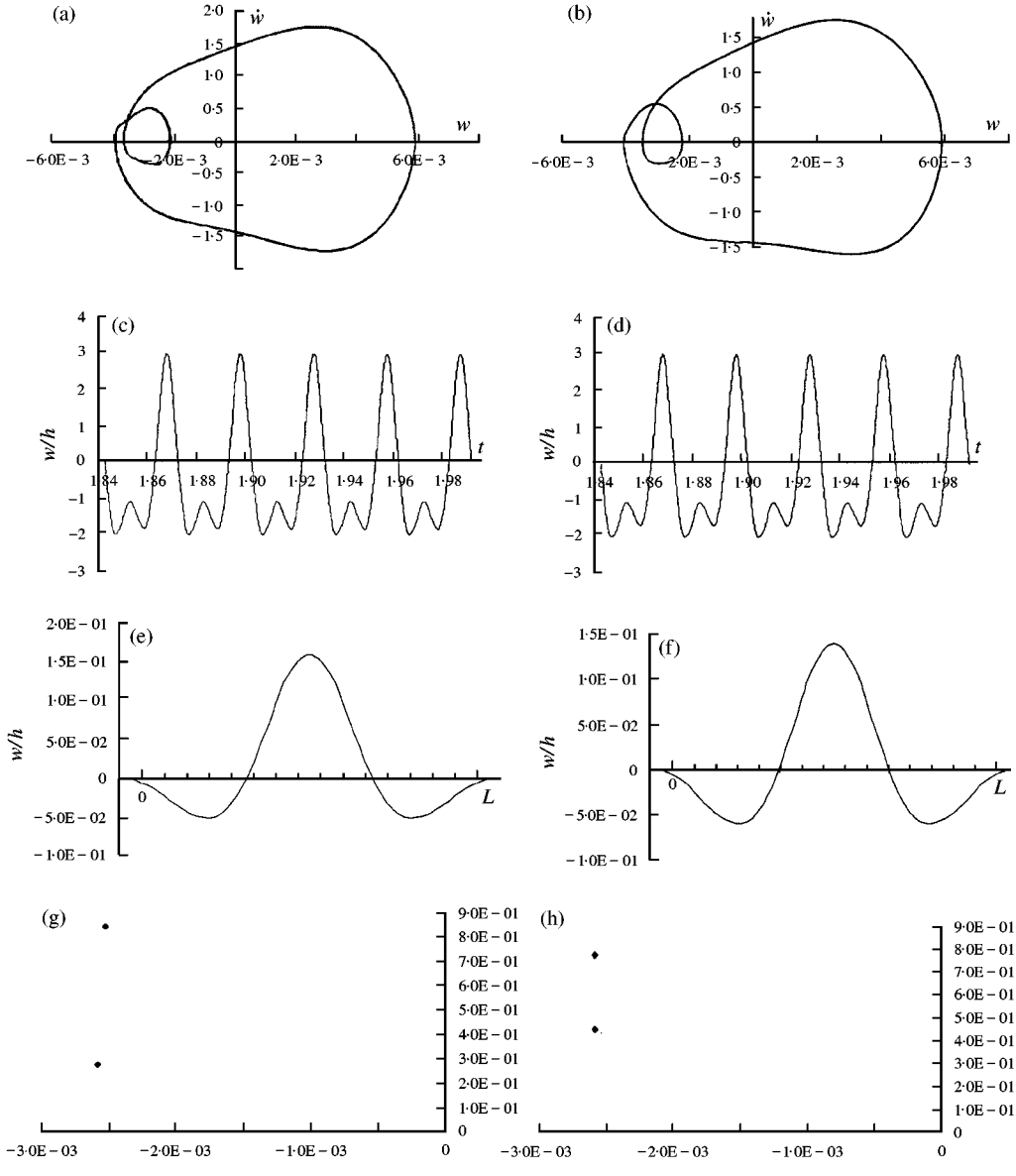

Figure 5. (a, b) Phase plots, (c, d) time histories, (e, f) shape assumed by the beam and (g, h) Poincaré maps. $F = 10$ N.

The phase plot is not a closed curve; therefore the response is not periodic. The time history of the response has a random aspect, characteristic of motions with many frequency components. The period of the first forcing term is $T = 2\pi/\Omega$, where Ω is 210 rad/s. This period was used to construct the Poincaré map by starting at $t = 0$ and sampling the state variables—displacement and velocity—at intervals T [20, 28]. It appears that the Poincaré map is neither a closed curve, nor a number of discrete points and therefore the motion may be chaotic.

An excitation with a constant term and a harmonic term with a frequency close to the fifth natural frequency, $F = 5000(1 + \cos(5200t))$, was applied transversely at a quarter of

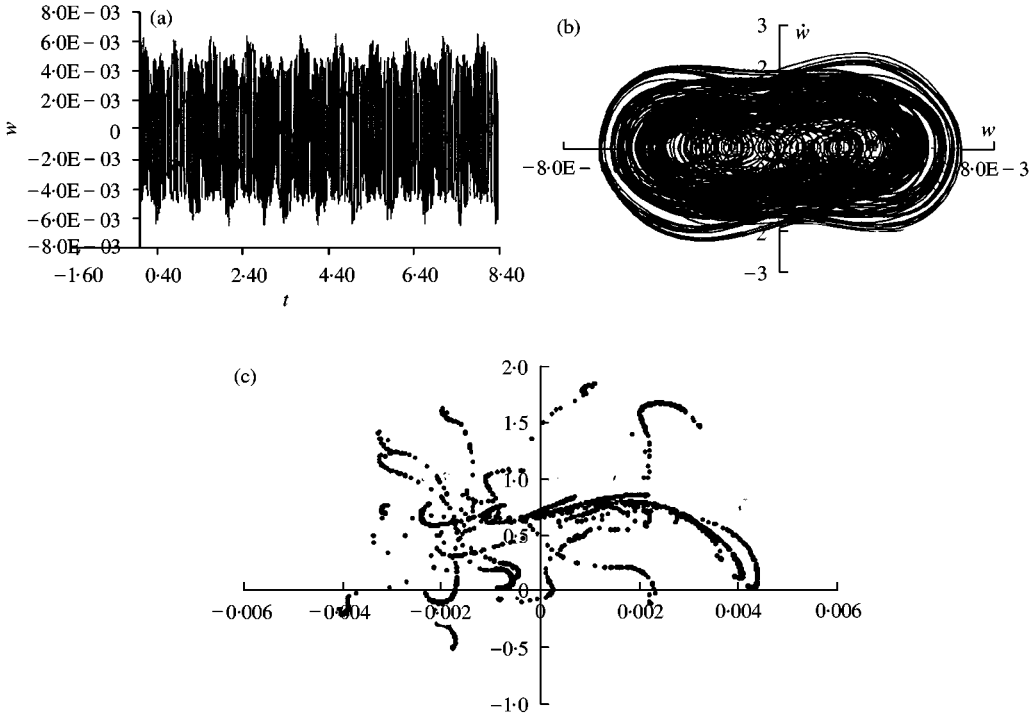

Figure 6. (a) Time history, (b) phase plane and (c) Poincaré map.

bar 2 of Frame 1. Figure 7 shows the respective phase plot, time history and Poincaré map of the transverse displacement at a quarter of beam 2. The Poincaré map was defined by sampling the system at intervals of $2\pi/5200$ s. The frequency of excitation is close to the fifth linear natural frequency. Nevertheless, with the hierarchical finite element model used, which has only 39 d.o.f., it is possible to study very high order modes of vibration.

By analyzing the mode shapes it was found that the response is modulated by the second and fifth modes. However, since the phase plot is a closed line and the orbit defines a point in the Poincaré section, the response is periodic. The motion presents beating, but the beating frequency is 3900 rad/s and is commensurate with 5200 rad/s ($3 \times 5200 - 4 \times 3900 = 0$), which confirms the periodicity of the response.

A transverse excitation with the form $5000(\cos(2400t) + \cos(2600t))$ was applied at a quarter of bar 2 of Frame 1. Figure 8 shows the phase plot, time history and Poincaré map of the transverse displacement at a quarter of beam 2. The phase plot is a closed line, but with several loops. The Poincaré section—which was defined by sampling the system at intervals of $2\pi/2400$ s—is a finite number of discrete points. Therefore, the response is still periodic, but several period-doubling bifurcations occurred.

5. CONCLUSIONS

Several sets of displacement shape functions for hierarchical beam elements were investigated. In general, geometrically non-linear plane problems, regarding the transverse displacement shape functions, Legendre polynomials plus Hermite cubics have more advantages than the beam eigenfunctions and trigonometric functions investigated. With

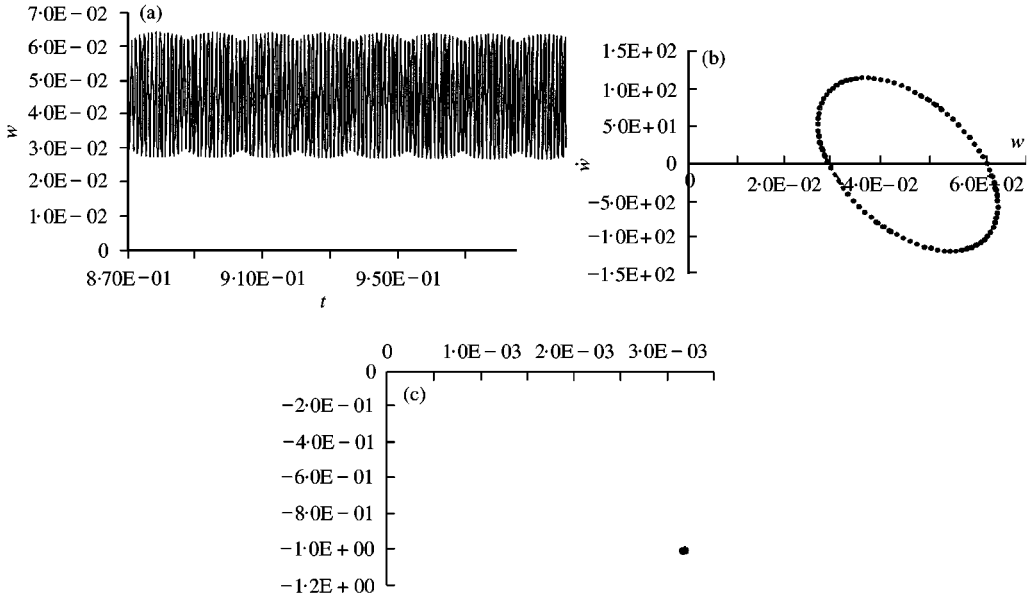

Figure 7. (a) Time response, (b) phase plot and (c) Poincaré map at point $\xi = 0{\cdot}5$ of bar 2.

those polynomials accuracy is achieved with a small number of degrees of freedom, C^1 continuity is guaranteed between elements, and the element matrices are quickly derived. For a general plane problem, the g polynomials plus linear functions are recommended as axial displacement shape functions for beam elements. Sine functions are recommended for both transverse and axial displacements for beam elements with simply supported boundary conditions. Another good option for this last case is the set of g polynomials.

Time domain analyses of beams and frames were carried out using hierarchical finite element spatial models. Due to the small number of degrees of freedom characteristic of this method, it was possible to obtain quickly the response in the time domain, and to collect sufficient data to define Poincaré sections, and to study periodic and non-periodic motions involving several modes. Therefore, the HFEM is an efficient tool for geometrically non-linear analyses in the time domain.

ACKNOWLEDGMENTS

The author gratefully acknowledges the help of Ms Luísa Silva and Mr Robertt Valente with the commercial FEM package, the referee's suggestions, and the partial support of this work by the Portuguese Science and Technology Foundation under project POCTI/1999/EME/32641.

REFERENCES

1. N. S. BARDELL 1991 *Journal of Sound and Vibration* **151**, 263–289. Free vibration analysis of a flat plate using the hierarchical finite element method.
2. W. HAN and M. PETYT 1996 *Computers and Structures* **61**, 705–712. Linear vibration analysis of laminated rectangular plates using the hierarchical finite element method—I: Free vibration analysis.

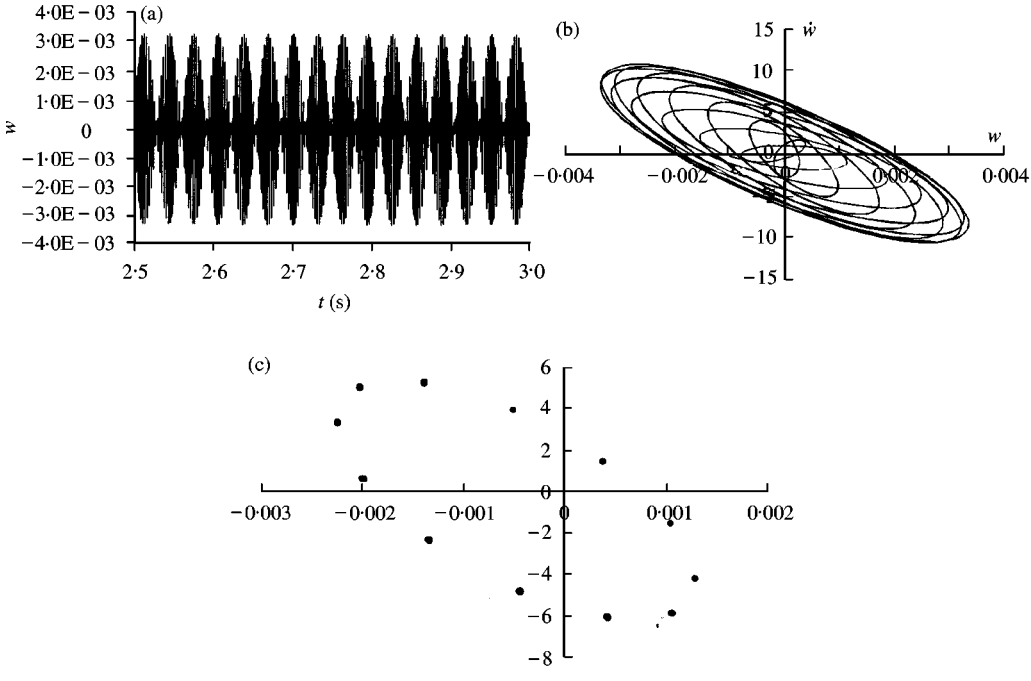

Figure 8. (a) Time response, (b) phase plot and (c) Poincaré map at point $\xi = 0{\cdot}5$ of bar 2.

3. W. HAN and M. PETYT 1996 *Computers and Structures* **61**, 713–724. Linear vibration analysis of laminated rectangular plates using the hierarchical finite element method—II: Forced vibration analysis.
4. W. HAN and M. PETYT 1997 *Computers and Structures* **63**, 295–308. Geometrically nonlinear vibration analysis of thin, rectangular plates using the hierarchical finite element method—I: The fundamental mode of isotropic plates.
5. W. HAN and M. PETYT 1997 *Computers and Structures* **63**, 309–318. Geometrically nonlinear vibration analysis of thin, rectangular plates using the hierarchical finite element method—II: 1st mode of laminated plates and higher modes of isotropic and laminated plates.
6. P. RIBEIRO and M. PETYT 1999 *International Journal of Mechanical Sciences* **41**, 437–459. Nonlinear vibration of plates by the hierarchical finite element and continuation methods.
7. P. RIBEIRO and M. PETYT 1999 *Composite Structures* **46**, 197–208. Nonlinear vibration of composite laminated plates by the hierarchical finite element method.
8. P. RIBEIRO and M. PETYT 1999 *Journal of Sound and Vibration* **224**, 591–624. Non-linear vibration of beams with internal resonance by the hierarchical finite element method.
9. L. J. WEST, N. S. BARDELL, J. M. DUNSDON and P. M. LOASBY 1997 in *Structural Dynamics: Recent Advances* (N. S. FERGUSON, H. F. WOLFE and C. MEI, editors), 217–227. Southampton: The Institute of Sound and Vibration Research. Some limitations associated with the use of k-orthogonal polynomials in hierarchical versions of the finite element method.
10. A. HOUMAT 1997 *Journal of Sound and Vibration* **206**, 201–215. An alternative Hierarchical finite element formulation applied to plate vibrations.
11. A. Y. T. LEUNG and J. K. W. CHAN 1998 *Journal of Sound and Vibration* **212**, 179–185. Fourier p-element for the analysis of beams and plates.
12. O. BESLIN and J. NICOLAS 1997 *Journal of Sound and Vibration* **202**, 633–655. A hierarchical functions set for predicting very high order plate bending modes with any boundary conditions.
13. N. S. BARDELL, J. M. DUNSDON and R. S. LANGLEY 1998 *Journal of Sound and Vibration* **217**, 297–320. Free vibration of thin, isotropic, open, conical panels.

14. R. LEWANDOWSKI 1994 *Journal of Sound and Vibration* **170**, 577–593. Non-linear free vibrations of beams by the finite element and continuation methods.
15. M. PETYT 1990 *Introduction to Finite Element Vibration Analysis*. Cambridge: Cambridge University Press.
16. S. H. CRANDALL 1970 *Journal of Sound and Vibration* **11**, 3–18. The role of damping in vibration theory.
17. Y. K. CHEUNG and S. L. LAU 1982 *Earthquake Engineering and Structural Dynamics* **10**, 239–253. Incremental time–space finite strip method for non-linear structural vibrations.
18. T. J. MENTEL 1959 in *Colloquium on Structural Damping* (J. E. Ruzicka, editor), 89–116. New York: The American Society of Mechanical Engineers. Vibrational energy dissipation at structural support junctions.
19. P. RIBEIRO 2001 *Computers and Structures* **79**, 107–117. The second harmonic and the validity of Duffing's equation for vibration of beams with large displacements.
20. A. H. NAYFEH and B. BALACHANDRAM 1995 *Applied Nonlinear Dynamics: Analytical, Computational, and Experimental Methods*. New York: John Wiley and Sons.
21. M. A. CRISFIELD 1997 *Non-linear Finite Element Analysis of Solids and Structures*. Chichester: John Wiley & Sons.
22. C. M. HARRIS 1988 *Shock and Vibration Handbook*. New York: Mc Graw-Hill; third edition.
23. B. S. SARMA and T. K. VARADAN 1983 *Journal of Sound and Vibration* **86**, 61–70. Lagrange-type formulation for finite element analysis of non-linear beam vibrations.
24. S. WOINOWSKI-KRIEGER 1950 *American Society of Mechanical Engineers Journal of Applied Mechanics* **17**, 35–36. The effect of an axial force on the vibration of hinged bars.
25. J. N. REDDY and I. R. SINGH 1981 *International Journal for Numerical Methods in Engineering* **17**, 829–852. Large deflections and large-amplitude free vibrations of straight and curved beams.
26. R. B. BHAT 1985 *Journal of Sound and Vibration* **102**, 493–499. Natural frequencies of rectangular plates using characteristic orthogonal polynomials in Rayleigh–Ritz method.
27. P. RIBEIRO and M. PETYT 1995 *Institute of Sound and Vibration Research Technical Memorandum* 773. Study of nonlinear free vibration of beams by the hierarchical finite element method.
28. K. YAGASAKI 1995 *Journal of Sound and Vibration* **183**, 1–31. Bifurcations and chaos in a quasi-periodically forced beam: theory, simulation and experiment.

APPENDIX A: DISPLACEMENT SHAPE FUNCTIONS

A.1. *f* DISPLACEMENT SHAPE FUNCTIONS

The first four *f* displacement shape functions are the Hermite cubics:

$$f_1 = \tfrac{1}{2} - \tfrac{3}{4}\xi + \tfrac{1}{4}\xi^3, \quad f_2 = \tfrac{1}{4} - \tfrac{1}{4}\xi - \tfrac{1}{4}\xi^2 + \tfrac{1}{4}\xi^3,$$

$$f_3 = \tfrac{1}{2} + \tfrac{3}{4}\xi - \tfrac{1}{4}\xi^3, \quad f_4 = -\tfrac{1}{4} - \tfrac{1}{4}\xi + \tfrac{1}{4}\xi^2 + \tfrac{1}{4}\xi^3.$$

The other *f* shape functions are the Rodrigues form of Legendre polynomials, given by

$$f_r = \sum_{n=0}^{INT(r/2)} \frac{(-1)^n(2r-2n-7)!!}{2^n n!(r-2n-1)!}\,\xi^{r-2n-1}, \quad r > 4,$$

where $r!! = r(r-2)\ldots(2 \text{ or } 1)$, $0!! = (-1)!! = 1$ and INT($r/2$) denotes the integer part of $r/2$.

A.2. *g* DISPLACEMENT SHAPE FUNCTIONS

The first two *g* shape functions are linear functions,

$$g_1 = \tfrac{1}{2} - \tfrac{1}{2}\xi, \quad g_2 = \tfrac{1}{2} + \tfrac{1}{2}\xi$$

and the following are given by

$$g_r = \sum_{n=0}^{INT(r/2)} \frac{(-1)^n (2r-2n-5)!!}{2^n n!(r-2n-1)!} \xi^{r-2n-1}, \quad r > 2.$$

A.3. TRIGONOMETRIC SHAPE FUNCTIONS

The set trigonometric shape functions is defined by the following equation:

$$t_r = \sin\left((r-4)\frac{\pi}{2}(\xi+1)\right)\sin\left(\frac{\pi}{2}(\xi+1)\right), \quad r > 4.$$